Water-Pumping Permanent Magnet Synchronous Motor Optimization Based on Customized Torque-Speed Operating Area and Performance Characteristics

Carlos Candelo-Zuluaga
MCIA Research Group (UPC)
Terrassa, Spain
carlos.andres.candelo@upc.edu

Antonio Garcia Espinosa
MCIA Research Group (UPC)
Terrassa, Spain
garciae@ee.upc.edu

Jordi-Roger Riba
MCIA Research Group (UPC)
Terrassa, Spain
riba@ee.upc.edu

Pere Tubert Blanch
Midtal talentos S.L.
Banyoles, Spain
pere.tubert@midtal.net

Francesc Jiménez Descalzo
Midtal talentos S.L.
Banyoles, Spain
francesc.jimenez@midtal.net

***Abstract*—This paper presents a novel methodology for optimizing Permanent Magnet Synchronous Motors for Water-Pumping applications. The algorithm is designed to start the optimization process from a predefined torque-speed area, its desired envelope, and the performance characteristics of the motor to be obtained after the optimization process, providing the information in an efficiency map, according to a predefined control strategy (MTPA, MTPV, etc.). This work also implements an image comparison technique based on the structural similarity index to evaluate the objective function.**

Keywords—electric machines optimization, permanent magnet synchronous motor drives, water pump, structural similarity index.

I. INTRODUCTION

For water-pumping applications, so far, the induction motor has been the most applied electrical motor topology, usually conceived to operate in a single operating point in the torque-speed map. Nevertheless, nowadays water-pumping applications are increasingly requiring motors capable to operate in different torque-speed regions, and thus, being able to adapt their operating conditions for variable pressure and volumetric flow demands [1],[2].

Most of the works found in the technical literature focused on motor optimization, are based on settling the main characteristics (rated power and speed, power factor and voltage among others) and by defining an objective function based on a single operational point in the torque-speed plane [3], or considering multiple operating points from the driving cycle [4],[5] but without specifying the overall map magnitudes, gradients in the maps and envelopes of the physical parameters to study.

For this reason, when designing an electric motor for such applications, it is not only important to define appropriately the rated characteristics, but also the properties of the operating region that optimizes the whole system efficiency.

Thus, with the new design demands, some new design constraints are required in each of the components of the water pumping system. Focusing on the motor part, the new design targets are the cost and volume reduction, and increase the whole system reliability and efficiency.

Moreover, this motor design approach can take into account both, the main working area and the region of maximum efficiency of the pump, thus resulting in a completely optimized pumping system.

In this context, it is necessary to propose a design and optimization method that takes into account not only the rated conditions, but at the same time being capable to optimize multiple frequent operating points placed in the torque-speed plane.

The methodology presented in this study deals with the motor behaviour maps [6]–[9]. It allows to represent on a map the magnitude, distribution and limits of a physical parameter within the torque-speed region.

The paper is organized as follows. Section II presents the optimization process based on the behaviour maps. Section III details the optimization parameters and the treatment applied. Section IV presents the magnetic model. Section V exposes the comparison method used to build the optimization objective function to be minimized by means of the Structural Similarity Index (SSIM) [10], [11]. Section VI shows and discusses the results. Finally, the conclusions are summarized in Section VI.B.

II. BEHAVIOUR MAP OPTIMIZATION PROCESS

The first step consists in determining the torque and speed requirements of the motor drive from the hydraulic efficiency, input power and characteristic pump curve versus the volumetric flow of the pumping system.

Fig. 1 shows the hydraulic efficiency map of the pump in per unit magnitude, which have been scaled by the rated working point of the pump. Then, all the values presented in this study are scaled by means of this torque and speed point.

Once the hydraulic efficiency map is determined from the aforesaid data, it is possible to localize the most suitable working region of the pump. Therefore, it is necessary to design the optimal motor characteristics to operate within the interest region, which has to match with the lower cost and the maximum overall system efficiency.

978-1-7281-4878-6/19/$31.00 ©2019 IEEE

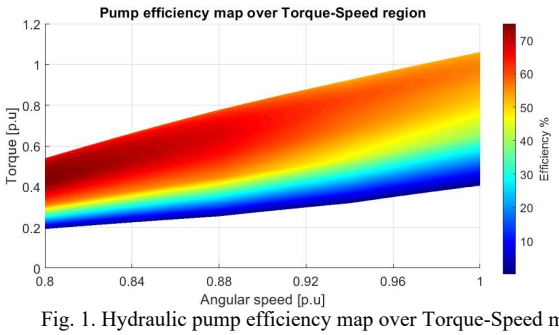

Fig. 1. Hydraulic pump efficiency map over Torque-Speed map

Fig. 2 shows a generic example, determining the working region of interest and showing three different motor envelopes that could be analysed during the design process.

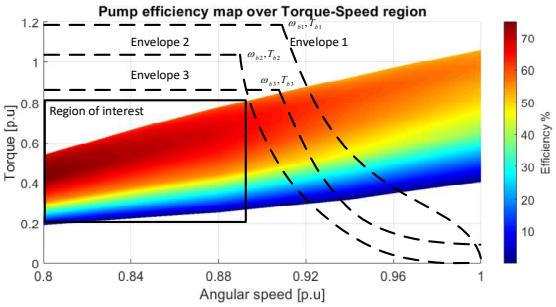

Fig. 2. Hydraulic pump efficiency map over Torque-Speed map with generic feasible envelopes and with the region of interest determined.

The motor optimization methodologies found in the literature do not present a complete control over the motor target characteristics and the overall behavior map distribution. For this reason, this study proposes a novel method that takes into account not only the rated conditions, but also the region of interest predefining some performance characteristics such as efficiency, power factor, or current control commands according a predefined control strategy (MTPA or MTPV), among others. When predefining the behavior maps [6]–[9] during the initial design stage, they implicitly take into account the motor information such as the direct to quadrature inductance ratio, flux linkage or stator resistance among others. Thus, the optimization process starts by defining the initial constraints, including the behavior maps, boundary conditions (main geometric dimensions, DC bus voltage, maximum speed, etc.), and finds the optimal geometry and characteristics matching with the initial constraints.

The Structural Similarity Index (SSIM) [10], is used as a quality index to determine whether the optimized geometry matches with the objective maps. The SSIM returns a normalized number in the range 0 and 1 to express the degree of similarity between two matrices taking into account three main aspects, i.e., the point by point difference, the whole standard deviation and the structural similarity. This method is explained in detail in Section V.

A. *Optimization Approach*

The optimization approach proposed in this paper is divided in three sub-processes, i.e., the electromagnetic pre-design, optimization and motor validation processes.

1) Electromagnetic Pre-Design process

The first step consists in calculating a seed or starting point of the geometry by using analytical equations. To this end some input parameters must be settled, for instance the predicted power requirement, and some constraints such as the DC bus voltage, number of phases, number of poles or rotor topology.

2) Optimization algorithm process

Once the Pre-Design process provides the seed geometry and the motor parameters, an optimization process within the torque-speed plane is performed. The objective is to maximize the SSIM [10] of the behaviour maps with respect to the objective maps.

3) Motor validation

Finally, the geometry obtained from the optimization process is validated by means of Finite Element Analysis (FEA).

The whole process is shown in Fig. 3. The algorithm is described more in depth in the next subsection.

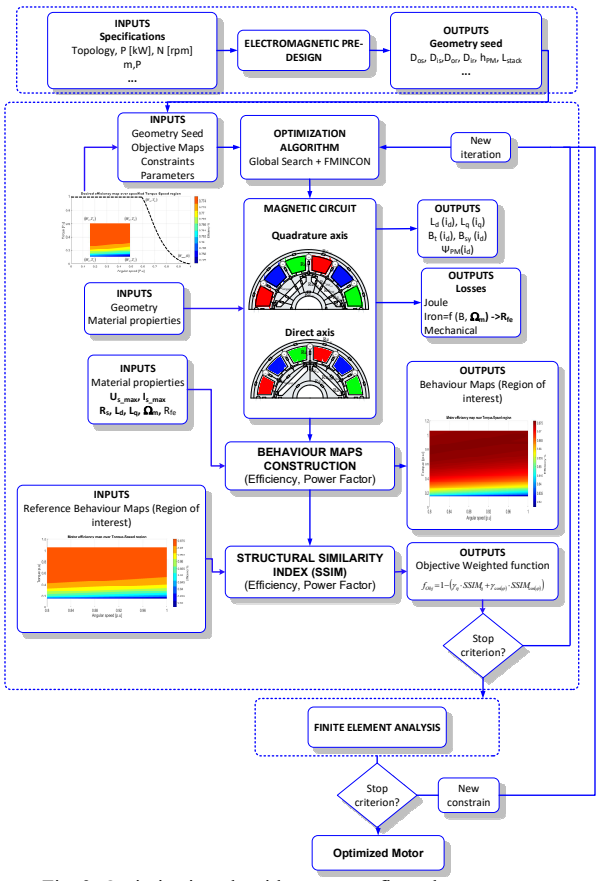

Fig. 3. Optimization algorithm process flow chart

B. *Optimization Algorithm Process*

The optimization algorithm process is composed of five main sub-processes. The data structure creator, optimization solver, the magnetic circuit evaluation, the motor behaviour maps calculation and finally in order to analyze the objective function, the structural similarity index (SSIM).

1) Data Structure Creator

At first, the seed geometry and parameters provided by the

predesign process are considered. This first approach is designed first, following analytical equations and posteriorly is verified with finite element analysis to guarantee that its performance is nearby the target.

On the other hand, it is integrated the optimization region within the torque-speed map to be optimized, the target behaviour maps, the parameter bounds and laws to satisfy in every optimization iteration must be settled beforehand.

This process takes all input information and builds a data structure.

2) Optimization Solver

Once the data structure is built, an optimization solver must be selected. Within the solvers available in the Global Optimization Toolbox™ of MATLAB®, this study deals with the Global Search tool and the FMINCON solver using the Interior Point algorithm. Thus, within the specified constraints, it is possible to generate a multiple initial population and to evaluate the global minima with the given constraints.

3) Magnetic Circuit Evaluation

Once selected the optimization solver, the algorithm calculates the behaviour maps. The first evaluation is the magnetic circuit with the geometry proposed by the solver. Then, the direct and quadrature axis inductances, the permanent magnet flux linkage and the flux density in the stator teeth and yoke over the feeding stator current, are found. Thus, when calculating the motor behaviour maps, these magnitudes are discretized in the torque-speed domain.

The magnetic circuit evaluation procedure is explained in detail in section IV.

4) Motor Behaviour Maps

The fourth sub-process during the optimization algorithm loop is the calculation of the motor behaviour maps. At this point the type of control must be settled within the following options,

- Field oriented control (FOC) with Maximum Torque per Ampere (MTPA) and Flux Weakening (FW).
- Field Oriented Control (FOC) with Maximum Torque per Ampere (MTPA) region.
- Quadrature axis current injection.

Once the control is specified, the maps are calculated following the electrical model in the direct and quadrature axes with the electromagnetic torque equation. The winding losses are modelled by means of a series resistance and the magnetic losses by means of a parallel resistance [12].

The Electromagnetic torque equation is as,

$$T = \frac{m}{2} \cdot p \cdot \left[\Psi_{PM} \cdot i_{od} + \left(L_d - L_q \right) \cdot i_{od} \cdot i_{oq} \right] \tag{1}$$

Whereas the voltage equations:

$$u_d = R_s \cdot i_d + L_d \cdot \frac{d}{dt} \cdot i_{od} - \omega_m \cdot L_q \cdot i_{oq} \tag{2}$$

$$u_q = R_s \cdot i_q + L_q \cdot \frac{d}{dt} \cdot i_{oq} + \omega_m \cdot L_d \cdot i_{od} + \omega_m \cdot \Psi_{PM} \tag{3}$$

The stator current is defined as the sum of the current consumed in the iron resistance and the current due to the motor demand.

$$\begin{cases} i_d = i_{cd} + i_{od} \\ i_q = i_{cq} + i_{oq} \end{cases} \tag{4}$$

To compute the power balance, the system losses in the direct and quadrature axes are defined.

$$P_{Cu} = \frac{m}{2} \cdot \left({i_d}^2 + {i_q}^2 \right) \cdot R_s \tag{5}$$

$$P_{Fe} = \frac{m}{2} \cdot \left({i_{cd}}^2 + {i_{cq}}^2 \right) \cdot R_{Fe} \tag{6}$$

$$P_{mech} = k_{mech} \cdot {\Omega_m}^3 \tag{7}$$

As can be observed, there are three types of losses in the system, the losses from the winding resistance, the magnetic losses in the steel laminations and the mechanical losses.

The input and output power in direct and quadrature axis model are defined as,

$$P_{in} = \frac{m}{2} \cdot \left(u_d \cdot i_d + u_q \cdot i_q \right) \tag{8}$$

$$P_{out} = T \cdot \Omega_m \tag{9}$$

5) Structural Similarity Index (SSIM)

Finally, once the behaviour maps are available, the structural similarity index (SSIM) [10] must be calculated. The SSIM condenses three different comparisons, i.e., luminance, contrast and structure. As this method was developed for image applications the term of luminance is translated to magnitude values, contrast to standard deviation and structure as the unit standard deviation of the data. The resulting SSIM value is normalized between 0 and 1, where 0 indicates minimum equality and 1 maximum equality.

The SSIM between each physical parameter calculated in a behaviour map and the target maps of the same magnitude is calculated. Therefore, the objective function to be minimized is built as the weighted sum of each SSIM.

For the sake of simplicity, the objective function considered in this study is based on the efficiency and power factor maps as follows,

$$f_{Obj} = 1 - \left(\gamma_\eta \cdot SSIM_\eta + \gamma_{\cos(\varphi)} \cdot SSIM_{\cos(\varphi)} \right) \tag{10}$$

Being γ_η and $\gamma_{\cos(\phi)}$ the weights assigned to the efficiency and power factor structural similarity index correspondingly.

III. Motor Parameters Optimization

The optimization process takes all the physical parameters specified in the first stage to find the optimal motor. The optimization parameters used to characterize the motor are summarized in TABLE I.

A. Geometry characterization

The geometry parameters are divided into the stator and rotor components. This parameterization is aimed to characterize the motor geometry using the minimum number of variables. Fig. 4 shows the geometry parameters of an Interior Permanent Magnet Synchronous Motor (IPMSM), which has selected to build the prototype.

The remaining geometry parameters are considered to be dependent, thus, reducing the amount of variables considered by the optimization solver.

B. Optimization parameters

Besides the high number of variables, some of them are interrelated. Thus, by applying suitable rules, the computational burden of the optimization process can be

greatly reduced. Since the electromagnetic predesign has been applied prior to the optimization process, the seed values of the parameters to be optimized are supposed to be close to the optimal values, thus allowing to reduce the upper and lower bounds of such parameters to accelerate the optimization process.

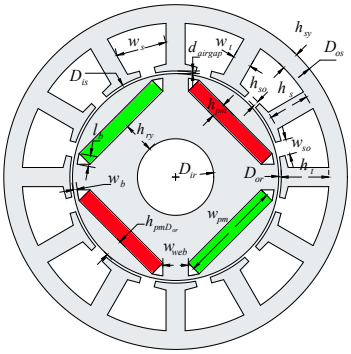

Fig. 4. Motor parametrization

TABLE I. OPTIMIZATION PARAMETERS LIST

Name	Parameter	Name	Parameter
Magnet Coverage	α_{PM}	Winding factor	K_w
Slot opening width	w_{so}	Stack Length	L
Airgap length	d_{airgap}	Bridge length	L_b
Inner rotor diameter	D_{ir}	Stator phases	m
Inner stator diameter	D_{is}	Number of phase turns	N_{ph}
Outer rotor diameter	D_{or}	Number of pair poles	p
Outer stator diameter	D_{os}	Number of slots per pole and phase	q
Permanent magnet height	h_{pm}	Number of slots	Q
Permanent magnet to outer rotor diameter distance	h_{pmDor}	Stator phase resistance	R_s
Rotor yoke height	h_{ry}	Maximum stator line voltage	U_{smax}
Slot height	h_s	Bridge width	w_b
Stator yoke height	H_{sy}	Permanent magnets width	w_{pm}
Tooth height	h_t	Slot width	W_s
Slot opening height	h_{so}	Tooth width	W_t
Maximum stator current	I_{smax}	Web width	W_{web}
Slot filling factor	K_u		

IV. MAGNETIC CIRCUIT EVALUATION

The magnetic model developed to evaluate the geometry proposed by the optimization algorithm is based on a reluctance network [9]. The aim of analyzing the magnetic circuit is to obtain the direct and quadrature axis inductances as a function of the stator current taking into account the iron saturation. Moreover, it is obtained useful information about the stator and rotor saturation required to compute the magnetic losses.

Fig. 5 and Fig. 6 show the quadrature and direct axis reluctance networks to determine the inductances.

The quadrature inductance is calculated by computing the flux linked by the phase aligned with the axis divided by the peak current circulating through it.

$$L_q = \frac{m}{2} \cdot 2 \cdot p \cdot N_{ph} \cdot \frac{\sum_{i=1}^{i=Q/(2\cdot p)} \phi_{q_i}}{I_q} \tag{11}$$

Being:

- m: The number of stator phases.
- p : The pole pairs.
- N_{ph} : The number of turns of a single phase.
- ϕ_{q_i} : The flux passing through the tooth i in quadrature axis.
- I_q : The quadrature axis current.

As observed, in order to take into account the saturation effects in the rotor, a reluctance is placed in the rotor web and on the bridge.

From the direct axis reluctance network, the inductance is computed as the linked flux created by the stator winding divided by the peak current circulating in the phase aligned with the axis of analysis.

$$L_d = \frac{m}{2} \cdot 2 \cdot p \cdot N_{ph} \cdot \frac{\sum_{i=1}^{i=Q/(2\cdot p)} \phi_{d\,i} - \phi_{PM_i}}{I_d} \tag{12}$$

Being:

$\phi_{d\,i}$: The *d*-axis flux passing through the tooth *i*-th.

$\phi_{PM\,i}$: The *d*-axis PM flux passing through the tooth *i*-th.

I_d : The *d*-axis current.

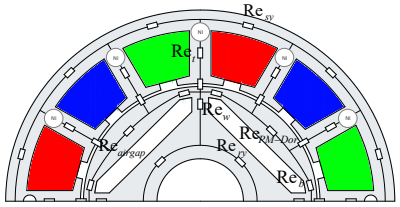

Fig. 5. Quadrature axis reluctance network

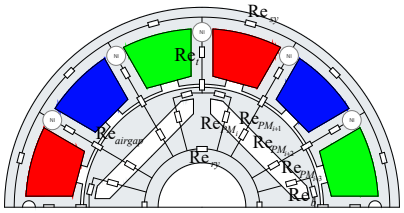

Fig. 6. Direct axis reluctance network

V. STRUCTURAL SIMILARITY INDEX (SSIM)

When comparing the behavior maps obtained through the electric and magnetic models with respect to the desired maps, it is important to discern three main aspects to study by means of matrix processing [10].

The first comparison between matrixes is defined as the mean intensities of both matrixes. The mean intensity of the reference matrix is defined as:

$$\mu_x = \frac{1}{N} \cdot \sum_{i=1}^{Ni} \sum_{j=1}^{Nj} x_{ij} \tag{13}$$

Being $N = Ni \cdot Nj$ the total number of components of the

matrix and x_{ij} the (i,j) component of the matrix. The comparison of the intensity (magnitudes) is given by:

$$l(x,y)=\frac{2\cdot\mu_x\cdot\mu_y+C_1}{\mu_x^{\,2}+\mu_y^{\,2}+C_1} \tag{14}$$

x and y being the matrices of study and C_1 is defined as a constant to avoid computational instabilities when $\mu_x^{\,2}+\mu_y^{\,2}$ is close to zero.

The second comparison is related to the difference of the standard deviation of each matrix. The standard deviation of the reference matrix is defined as,

$$\sigma_x=\left(\frac{1}{N-1}\cdot\sum_{i=1}^{Ni}\sum_{j=1}^{Nj}\left(x_{ij}-\mu_x\right)^2\right)^{\frac{1}{2}} \tag{15}$$

The comparison between the matrices standard deviation is given by,

$$c(x,y)=\frac{2\cdot\sigma_x\cdot\sigma_y+C_2}{\sigma_x^{\,2}+\sigma_y^{\,2}+C_2} \tag{16}$$

The third evaluation compares the normalized matrixes to analyse the data structure of each matrix.

The relation between the normalized matrixes $(X-\mu_x)/\sigma_x$ and $(Y-\mu_y)/\sigma_y$ is equivalent to the correlation coefficient between the matrices of study. Thus the structure comparison is defined by,

$$s(x,y)=\frac{\sigma_{xy}+C_3}{\sigma_x\cdot\sigma_y+C_3} \tag{17}$$

where σ_{xy} is the correlation coefficient between matrices:

$$\sigma_{xy}=\frac{1}{N-1}\cdot\sum_{i=1}^{Ni}\sum_{j=1}^{Nj}\left(x_{ij}-\mu_x\right)\cdot\left(y_{ij}-\mu_y\right) \tag{18}$$

The constant C_3 is defined as half of C_2 [10].

Finally, the SSIM results in,

$$SSIM=\left[l(x,y)\right]^{\alpha}\cdot\left[c(x,y)\right]^{\beta}\cdot\left[s(x,y)\right]^{\gamma} \tag{19}$$

Where the constants α,β,γ are set to unity [10].

VI. Results and Validation

The aim of this study is to show how by defining beforehand an efficiency map, it is possible to design and optimize a motor which matches with the pre-defined map. Thus, at first, the customized efficiency map to achieve during the optimization process is shown in Fig. 7.

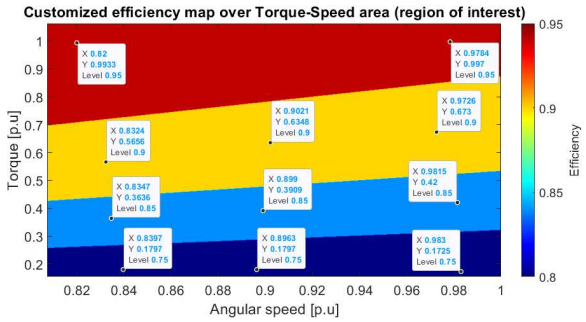

Fig. 7. Customized Torque-Speed motor efficiency map

As can be observed, four levels of efficiency (0.75, 0.85, 0.9 and 0.95) are defined.

After the optimization process, the following efficiency map is obtained from the optimization algorithm using reluctance networks.

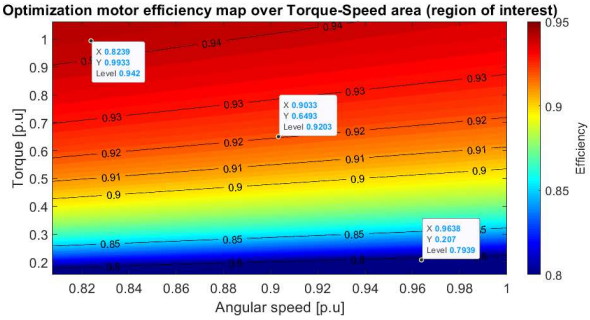

Fig. 8. Optimization reluctance network model Torque-Speed efficiency map

As can be observed, the gradients obtained are smoother than in the target map. That is due because the optimization process is based on the magnetic and electrical models, while adjusting as possible to the target map. Observing the data levels, a high similarity structure can be observed. That validates the optimization algorithm procedure, since the resulting map is finely adjusted to the target map.

To validate the motor parameters, the motor efficiency map in the region of interest is extracted by using FEA.

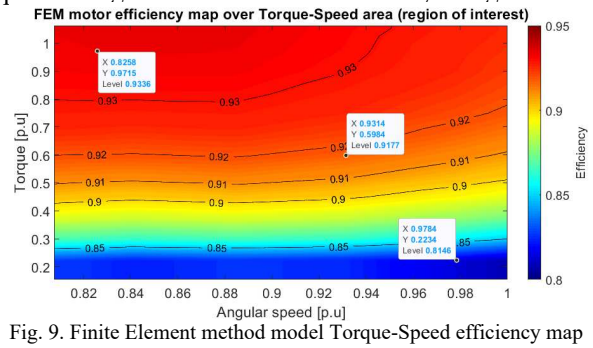

Fig. 9. Finite Element method model Torque-Speed efficiency map

As can be observed, the FEA torque-speed map validates the model results. The SSIM between FEA and reluctance network model is 0.993.

A. Efficiency map in whole area

In order to validate the model results, the whole efficiency map characteristics of the optimized motor is compared against the results obtained by applying FEA. Fig. 10 and Fig. 11 show the efficiency maps obtained from the optimization model and FEA, respectively.

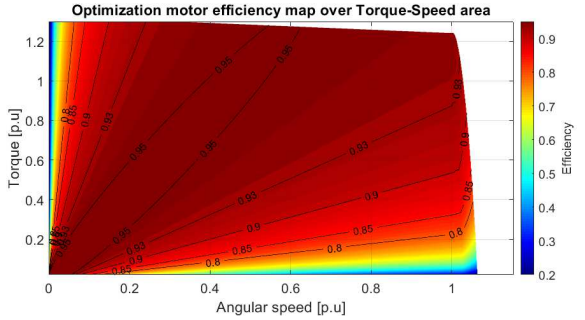

Fig. 10. Optimization model efficiency map in whole area

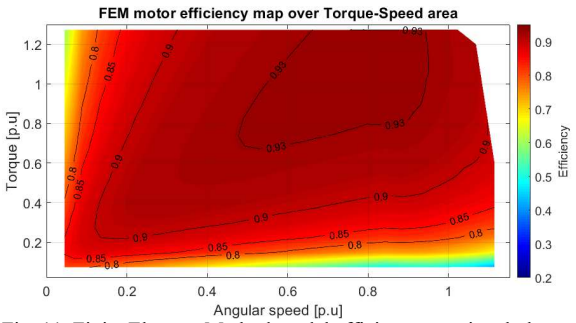

Fig. 11. Finite Element Method model efficiency map in whole area

As can be observed the model evaluates with high accuracy the overall motor performance. Nevertheless, in order to obtain better results, it is necessary to improve the electromagnetic model by considering the cross coupling effect and increasing the network resolution.

TABLE II. MOTOR CHARACTERISITICS

Features	**Value**
Rated speed (p.u)	1
Rated Torque (p.u)	1.275
Rated Current (A)	3
Rated Voltage (V)	200
Number of phases	3
Number of slots	9
Pole pairs	3
Slots/pole/phase (q)	0.5
Conductors per slot	160
Permanent magnets	Nd-35H
Magnetic steel	M440-50A
d-axis inductance (L_d,mH)	$4.9_{\text{no-load}}$-$4.0_{\text{rated-load}}$
q-axis inductance (L_q,mH)	$7.0_{\text{no-load}}$-$6.9_{\text{rated-load}}$

B. Computational burden

The optimization algorithm requires between 2.4-3.3 seconds for one iteration, this range depending on the iron saturation. The time required to find the optimum solution is about 4000 seconds. This result shows the computational viability of the method for a fast and reliable design and optimization tool. The number of candidates found by the solver was eleven, which required 11879 iterations during the last solver evaluation.

VII. CONCLUSIONS

This paper has presented a novel methodology to optimize a Permanent Magnet Synchronous Machines by defining the torque-speed area to achieve, the desired envelope and the performance characteristics providing the information in surface maps according a predefined control strategy.

The results have shown to be precise within the area of analysis with a high structural similarity index (0.993). Nevertheless, when representing the whole torque-speed region, the reluctance network model needs to be improved.

Regarding to the computational burden, the method has shown to be fast, reliable and precise. Despite of this, the method needs to be compared using other optimization solvers to increase its performance.

ACKNOWLEDGMENT

The authors would like to thank the support of the Generalitat de Catalunya under the Industrial Doctorate 2018DI004 and 2017SGR0967 projects, as well as the Spanish Ministry of Economy and Competitiveness under the project TRA2016-80472-R.

REFERENCES

[1] R. Antonello, M. Carraro, A. Costabeber, F. Tinazzi, and M. Zigliotto, "Energy-Efficient Autonomous Solar Water-Pumping System for Permanent-Magnet Synchronous Motors," *IEEE Trans. Ind. Electron.*, vol. 64, no. 1, pp. 43–51, Jan. 2017.

[2] A. Joseph, K. Desingu, R. R. Semwal, T. R. Chelliah, and D. Khare, "Dynamic Performance of Pumping Mode of 250 MW Variable Speed Hydro-Generating Unit Subjected to Power and Control Circuit Faults," *IEEE Trans. Energy Convers.*, vol. 33, no. 1, pp. 430–441, Mar. 2018.

[3] D. Fodorean, L. Idoumghar, M. Brevilliers, P. Minciunescu, and C. Irimia, "Hybrid Differential Evolution Algorithm Employed for the Optimum Design of a High-Speed PMSM Used for EV Propulsion," *IEEE Trans. Ind. Electron.*, vol. 64, no. 12, pp. 9824–9833, Dec. 2017.

[4] L. Dang, N. Bernard, N. Bracikowski, and G. Berthiau, "Design Optimization with Flux Weakening of High-Speed PMSM for Electrical Vehicle Considering the Driving Cycle," *IEEE Trans. Ind. Electron.*, vol. 64, no. 12, pp. 9834–9843, Dec. 2017.

[5] E. Carraro, M. Morandin, and N. Bianchi, "Traction PMASR Motor Optimization According to a Given Driving Cycle," *IEEE Trans. Ind. Appl.*, vol. 52, no. 1, pp. 209–216, Jan. 2016.

[6] C. Lopez-Torres, C. Colls, A. Garcia, J.-R. Riba, and L. Romeral, "Development of a Behavior Maps Tool to Evaluate Drive Operational Boundaries and Optimization Assessment of PMa-SynRMs," *IEEE Trans. Veh. Technol.*, vol. 67, no. 8, pp. 6861–6871, Aug. 2018.

[7] A. Mahmoudi, W. L. Soong, G. Pellegrino, and E. Armando, "Efficiency maps of electrical machines," in *2015 IEEE Energy Conversion Congress and Exposition (ECCE)*, 2015, pp. 2791–2799.

[8] C. Lopez-Torres, A. Garcia, J.-R. Riba, G. Lux, and L. Romeral, "Computationally Efficient Design and Optimization Approach of PMa-SynRM in Frequent Operating Torque–Speed Range," *IEEE Trans. Energy Convers.*, vol. 33, no. 4, pp. 1776–1786, Dec. 2018.

[9] C. Lopez-Torres, A. Garcia Espinosa, J.-R. Riba, and L. Romeral, "Design and Optimization for Vehicle Driving Cycle of Rare-Earth-Free SynRM Based on Coupled Lumped Thermal and Magnetic Networks," *IEEE Trans. Veh. Technol.*, vol. 67, no. 1, pp. 196–205, Jan. 2018.

[10] Z. Wang, A. C. Bovik, H. R. Sheikh, and E. P. Simoncelli, "Image Quality Assessment: From Error Visibility to Structural Similarity," *IEEE Trans. Image Process.*, vol. 13, no. 4, pp. 600–612, Apr. 2004.

[11] K. Ma, Z. Duanmu, H. Yeganeh, and Z. Wang, "Multi-Exposure Image Fusion by Optimizing A Structural Similarity Index," *IEEE Trans. Comput. Imaging*, vol. 4, no. 1, pp. 60–72, Mar. 2018.

[12] C. Lopez-Torres, G. Bacco, N. Bianchi, A. G. Espinosa, and L. Romeral, "A Parallel Analytical Computation of Synchronous Reluctance Machine," in *2018 XIII International Conference on Electrical Machines (ICEM)*, 2018, pp. 25–31.